J. Braz. Chem. Soc., Vol. 18, No. 3, 611-621, 2007.
Printed in Brazil - ©2007 Sociedade Brasileira de Química
0103 - 5053 $6.00+0.00

Article

Molecular Dynamics Study of the Differences in the Human Defensin Behavior near a Modelled Water/Membrane Interface

*Adriana M. Namba, Marcos R. Lourenzoni and Léo Degrève**

Departamento de Química, Faculdade de Filosofia Ciências e Letras de Ribeirão Preto, Universidade de São Paulo, Av. Bandeirantes, 3900, 14040-901 Ribeirão Preto-SP, Brazil

O comportamento das defensinas humanas HNP-1, HNP-2 e HNP-3 é estudado em um modelo de interface H_2O/CCl_4 por simulações de dinâmica molecular. O comportamento distinto do HNP-3, quando comparado ao dos HNP 1 e 2, pode ser associado ao fato de o HNP-3 ser a menos potente das três defensinas, uma vez que seus resíduos apolares, que poderiam atacar as membranas celulares dos organismos patogênicos estão protegidos no interior do peptídeo. Três mecanismos encontrados na literatura propõem que a ação dos HNPs sobre membranas ocorra, principalmente, pela interação entre os seus resíduos polares e os da superfície da membrana. Esses modelos não explicam com clareza o papel da região hidrofóbica da membrana na manutenção da estrutura quaternária do dímero de HNP, quando em contato com o interior da membrana. O conhecimento do comportamento da estrutura dimérica no estágio inicial da penetração na membrana, considerando, principalmente, a natureza hidrofóbica dos HNPs, mostrou-se essencial para explicar as diferenças nas suas ações. Este trabalho contribui para o entendimento do mecanismo da ação antimicrobiana das defensinas.

Human defensins HNP-1, HNP-2 and HNP-3 behavior is studied in a membrane interface model H_2O/CCl_4 by molecular dynamics simulation. The distinct HNP-3 behavior, when compared to HNP 1 and 2, can be associated to the fact that HNP-3 is the least potent of the three defensins, since its apolar residues, which could attack the cellular membranes of the pathogenic organisms, are shielded in the inner region of the peptide. Three mechanisms were proposed to explain the HNP action on cellular membranes. These mechanisms are unable to enlighten the membrane hydrophobic part role for preserving the quaternary structure of the peptide when it is interacting with the inner part of the membrane. They suggest that the damaging is mainly caused by the interactions between the localized charges of the peptides with charges on the membrane surface. These models do not clearly explain what the hydrophobic region role is in the stabilization of the quaternary HNP structure, when it is interacting with a membrane. The understanding of how the HNP dimers structure is conserved at the first stages of the insertion into the membrane is fundamental to explain the different activities of the peptides. This work aims at contributing for the understanding of the mechanism of the defensins antimicrobial action.

Keywords: human defensin, membrane model, molecular dynamics, antimicrobial peptides

Introduction

Antimicrobial peptides are the most important elements of the innate immune defense against bacterial and fungal infections.[1-3] They are greatly diversified and possess distinct structural and functional features.[4] Owing to their varied properties in biological environments no general mechanism has been proposed for the overall biological activity of peptide antibiotics. However, it is well known that a large number of peptide antibiotics interact with cell membranes of both prokaryotic and eukaryotic cells by disturbing the membrane integrity through pore formation and cell lysis, leading to cell death.[5-8] The groups of antimicrobial peptides that contain six cysteines have been classified as defensins.[9] Human neutrophil peptides (HNPs) 1, 2 and 3 are the three most abundant forms of human α-defensins constituting 30-50% of the protein contents of human azurophil granules and 5-7% of the neutrophil's total cellular protein contents.[10] They are composed of 29 (HNP-2) or 30 (HNP-1 and

*e-mail: leo@obelix.ffclrp.usp.br

HNP-3) amino acids, differing in sequence by only a single N-teminus residue.[11] The HNPs primary sequences are displayed in the Figure 1. The HNP-1 and HNP-3 three-dimensional structures have been elucidated by NMR[7] and X-ray experiments,[13] respectively. They are dimers composed by two asymmetric monomers (henceforth denoted by mon 1 and mon 2), being each one formed by a hydrogen-bonded pair of antiparallel β-strands connected by a short turn forming a β-hairpin.[14] Each monomer of HNP-3 is composed by eleven residues with polar side-chain, four of them (Arg6, Arg15, Arg16 and Arg25) are positively, two (Glu14 and Asp2) negatively charged and five (Tyr4, Tyr17, Tyr22, Thr19 and Gln23) are non-charged. The residues comprising the β-strands and the turns are indicated in the Figure 1. The HNP-3 dimer has the shape of a basket that is, partially, flattened at the top.[13] The bottom of the basket is hydrophobic, whereas the top contains polar side chains as well as the N- and C-termini of both monomers.[13] The methylene groups of some of the eight arginines contribute to the hydrophobic surface, while the charged guanidine ends form a ring around the dimer.[13]

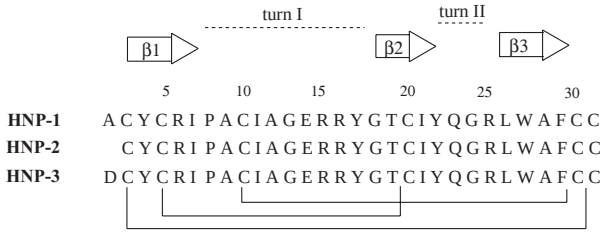

Figure 1. Primary sequence of HNP-1, HNP-2 and HNP-3. The disulfide bridges are represented by solid lines. The turn and the β-strands regions are indicated by dashed lines and by arrows, respectively.

Although the HNPs possess structural similarities, their antimicrobial properties are distinct (Table 1). Most HNPs are active against both Gram-negative and Gram-positive bacteria, fungi, viruses and mycobacterium, while others are also active against protozoa and chlamydia. HNP-3 is less microbicidal than the HNPs 1 and 2 against most of the microbes tested. Modern studies show that the HNPs 1-3 suppresses *in vivo* the activity and the replication of the HIV-1 virus exhibiting a powerful therapeutic value in the AIDS treatment.[27,28,30] The great interest of α-defensins is their low harmfulness against human cells, suggesting that they would be promising candidates to new antibiotics with high therapeutic value.

Based upon the structural amphiphilicity of the HNP-3 dimer, Hill *et al.*[13] proposed three possible mechanisms for the defensin activity:

(i) Single defensin dimers act as a wedge to disrupt the packing of the lipids in the bilayer. In this model, the hydrophobic basket bottom of the HNP-3 dimer, including the Gly18, Cys20, Ile21, Gly24, Leu26, Trp27, Ala28 and Phe29 residues, is inserted into the hydrocarbon layer of one lipid monolayer while the polar groups of the basket top, comprising the Tyr4, Gly14 and Tyr17 residues, and the arginine arms (Arg6, Arg15 and Arg16), maintain contact with aqueous phase or ionized groups of the N and C-termini (Asp2 and Cys31). This is a trans membrane bundle;

(ii) A dimer of dimers spans the bilayer so that a small solvent channel, a called wormhole model, is formed between them consistently with the observation of a small solvent channel in the HNP-3 crystal structure through the top of the HNP-3 basket. The channel would be part of the polar interface between two dimers while the hydrophobic basket bottoms would face outward toward the bilayer of the membrane;

(iii) An annulus of dimers forms a large central pore. The dimers would also span the bilayer as in model 2, but with a rotated orientation such that the hydrophobic basket bottoms face outward, into the bilayer, with the polar basket tops lining a pore.

Table 1. The antimicrobial spectrum of HNP-1, HNP-2 and HNP-3

Peptide	Spectrum
HNP-1	G+, G-, Fungi, Protozoa, Envelope virus, Mycobacterium, Chlamydia,[15-28,29,30]
HNP-2	G+, G-, Fungi,Envelope virus, Mycobacterium, Chlamydia,[15-17,19,20,23,24,27,29]
HNP-3	G-, Fungi, Envelope virus, Mycobacterium,[15,16,19,20,23,27]

Wimley *et al.*[31] observed the permeabilization of large unilamellar vesicles, suggesting that HNP-2 can form pores with a diameter of approximately 25 Å, according by with the formation of an annulus of dimers proposed by Hill *et al.*[13]. The experimental studies have suggested that the dimeric structure of the defensins is kept when they are in contact with the bilayer.[32]

The available models for the HNP/membrane interaction do not attribute the role of the hydrophobic region of the membrane in the maintenance of the peptide structure inside the membrane. The aim of this paper is to identify how the membrane hydrophobic region helps to conserve the HNP dimer stability, identifying in this way the main factors that provide the distinct antimicrobial activities of the dimeric forms of the human defensins HNP-1, HNP-2 and HNP-3 in a membrane interface model. The present studies extend previous analyses about the structure and hydration of the HNP-3 developed,[33,34] showing a high solvent

accessibility of most of the residues, together with attractive interactions with water molecules.

In this work, we performed a molecular dynamics (MD) study of dimeric HNPs in a membrane interface model formed by CCl_4 and H_2O. The use of a biphasic H_2O/CCl_4 as a membrane model has been described by Guba and Kessler.[35] The membrane interface model mimics the hydrophilic/hydrophobic environment. This system represents the unordered fatty acid chain matrix and the neighboring polar phase, respectively. A simple two-phase system, H_2O/CCl_4, has been demonstrated to be a plausible membrane mimetic in MD simulations, reproducing both the proper orientation of amphiphilic and correct phase preference of lipophilic organic molecules.[35] Additionally, the same approach also has been applied to the study of a polyether antibiotic, monensin[36] and to the study of two neuropeptides, SP and SP-Y8[37] to explore the orientation, conformation, and depth of peptide penetration into either phase. The objective of the present study is to understand how the interactions between the inner part of the membrane, here mimicked by the CCl_4 phase, and the HNP dimers are able to contribute to the maintenance of the HNP quaternary structure and, consequently, to get some insight on the different HNP activities.

Methods

Molecular dynamics simulations

Explicit solvent MD simulations were carried out using an *ad hoc* program and the GROMOS96 force field.[38] Separate solvent boxes of water and carbon tetrachloride molecules were equilibrated previously. The dimensions of the cells were adjusted to produce the correct experimental densities of 0.997 kg L^{-3} for SPC water[39] and 1.594 kg L^{-3} for carbon tetrachloride. The two solvent cells were merged and the energy was minimized during 1.0 ns. The initial set of HNP-3 dimer atomic coordinates was obtained from X-ray crystallographic data (pdb code: 1DFN).[13] The starting structures for the HNP-1 and HNP-2 dimer were obtained from the mutation of the HNP-3 X-ray crystal structure because of the lack of the HNP-1 and HNP-2 structures in the pdb data bank. For the HNP-1, the side-chain of the Asp2 residue of the crystal structure was changed by the side-chain of the Ala residue and for HNP-2, the Asp2 residue of the HNP-3 was eliminated. All MD simulations were performed in the NVT ensemble, using the Verlet algorithm,[40] with application of periodic boundary conditions and minimum image convention.[41,42] The integration time step was 2.0 fs. The bond lengths were constrained to a fixed value by SHAKE algorithm.[43] A cut-off at 1.4 nm was applied together with a Poisson-Boltzmann generalized reaction field to take into account the long-range electrostatic interactions.[40] Chloride ions were introduced in the aqueous phase to preserve the local electro neutrality. Firstly, one molecule of HNP-3 was placed into the aqueous medium to perform the simulations. The solvation of the peptide polar groups together with the lack of charged or zwitterionic groups at the membrane interface makes difficult the migration of the peptides toward the interface. Therefore, the MD studies were performed inserting the HNP-3 dimer into the carbon tetrachloride medium, keeping the ions into the aqueous phase to reduce the energetic cost of the migration of the peptide to the interface. Initially, the movements of the peptide and the water molecules were kept congealed to reduce the instabilities due to the inclusion of HNP-3 into the CCl_4 phase in order to model correctly the interface. The HNP-3 peptide arrived at the interface after 1.3 ns. Minimal energy configurations were obtained adding one more 0.3 ns simulation relaxing all the system excepting the rigid peptide that conserve the same structure obtained from X-ray crystallographic data[13] The profile of the configurational energy for the interaction between HNP-3 and CCl_4 is shown in figure 2. This equilibrium position was used to begin all MD simulations of other two HNPs. The movements of the peptide and the water molecules were set free and the MD was continued at 298 K for 6.0 ns. The aqueous phases were composed by n_w water molecules (n_w = 6660, 6652 and 6670, for HNP-1, HNP-2 and HNP-3, respectively) and the hydrophobic phase by 1288 carbon tetrachloride molecules. The dimensions of the biphasic system were x= 5.9 nm, y= 5.9 nm and z= 11.8 nm. The coordinates were stored every 10.0 ps for subsequent analysis.

Structural aspects

The root mean square deviation (RMSD) reflects the conformational changes induced by the interface presence.

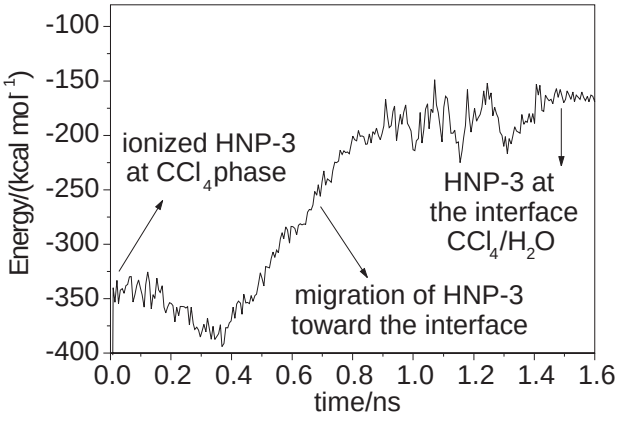

Figure 2. Configurational energy between CCl_4 and HNP-3.

It was used as mobility check using the reference conformation obtained from X-ray diffraction data.[13]

The main chain conformations of the amino acids were analyzed by ϕ and ψ angles, in agreement with the method proposed by Ramachandran and Sasisekharan.[44] The ϕ and ψ angles define the tilt between two neighboring amide planes (the plane of the peptide bond) with the C_α at the center of rotation. The values for these angles depend on the chemical nature of each one of the amino acids side-chains. The structure of the side-chains and the formation of hydrogen bonds (HB) between the hydrogen and oxygen atoms bonded to C and N atoms of C_α-C and N-C_α, respectively, are responsible for the formation of stable secondary structures. The maintenance of the secondary structures, in α-helical and β-sheet conformations, allows small oscillations of angles ϕ and ψ. The stability of each residue inside the structure can be measured through a statistic analysis of the angles obtained from the simulation trajectories. The standard deviations (σ, the square root of variance) of the ϕ and ψ dihedral angles were calculated for each residue.

Intramolecular hydrogen bonds

The intramolecular hydrogen bonds (HB_{i-i}) were identified using a geometric criterion: for all potential hydrogen bond, the distance between the donor (OH and NH) groups and the acceptor (oxygen atom) was monitored until a maximum of 2.35 Å. HB were accepted when the occurrence percentage was greater than 10%. Three types of HB_{i-i} were identified, including the HB_{i-i} involving a) the backbone atoms ($HB_{back-back}$), b) the backbone and the side-chain atoms '($HB_{back-side}$) and c) the side-chain atoms ($HB_{side-side}$).

Peptide-water interaction

The intermolecular hydrogen bonds with the water molecules (HB_{i-w}) were characterized using first the radial distribution functions g_i (r) between i atoms of HNPs and the oxygen or hydrogen atoms of the water molecules[41,45] and, second, the pair energy distributions, d_i (E),[45] where E is the configurational energy between the i atom and the water molecules. The numbers of water neighbors, N_w, in the first hydration shell of the peptide atoms, were obtained up to the first minimum of the g_i (r), $r_{min,1}$.[41,45] d_i (E) presents a peak, or a shoulder, in the region of intermolecular attractive interactions, specifically for $E \leq$ -5 kcal/mol, when the i of the peptide is hydrogen bonded with water. The peak area up to E_{min} gives the number of water molecules hydrogen bonded to the solute atom, $n_{i,HB}$, where E_{min} is the minimum energy.[45] Once the number of hydration is always larger than, or equal to, the number of hydrogen bonds, the next un-equality must be always respected: $n_{i,HB} \leq N_w$.

Results

Structure and flexibility of the peptides

RMSD for all backbone atoms between the starting structure and the simulated structures, expressing the changes in the conformation of the peptides at the biphasic interface along the 6.0 ns of simulations, are shown in Figure 3. During the thermalization, an increase of the RMSD is observed for all the three peptides. After 0.6 ns, an equilibrium state is reached for HNP-3, indicating a stabilized structure with RMSD of 0.32±0.04 nm. For HNP-1, the equilibrium state is reached after 1.6 ns, with a mean RMSD of 0.27 ± 0.06 nm. A significant increase in HNP-2 RMSD with time is observed (mean value of 0.36 ± 0.12 nm), indicating a major conformational variability for this defensin.

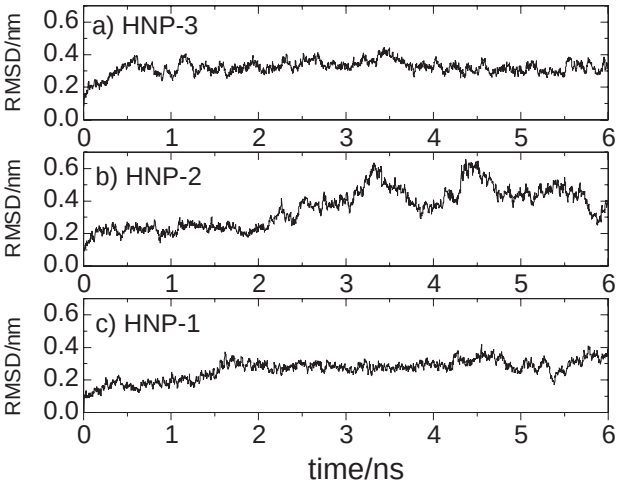

Figure 3. Root mean square deviations calculated over all the backbone atoms of the HNPs.

The standard deviations of the ϕ and ψ angles of each residue of the HNPs are displayed in Figure 4. High deviations are observed in the turn I region (Pro8 to Gly18), mainly in the mon 1. They obey the order: HNP-3 > HNP-2 > HNP-1. The turn I includes three structurally important residues for the mobility of the main chain: Pro8, Gly13 and Gly18. Higher deviations are observed for the residues located near the Gly13. Smaller oscillations are observed for the Gly24 that comprises the short turn (turn II) of the β-hairpin.

Intramolecular hydrogen bonds

Table 2 shows the HB_{i-i} detected in each monomer of HNPs, including $HB_{back-back}$, $HB_{back-side}$ and $HB_{side-side}$. The results

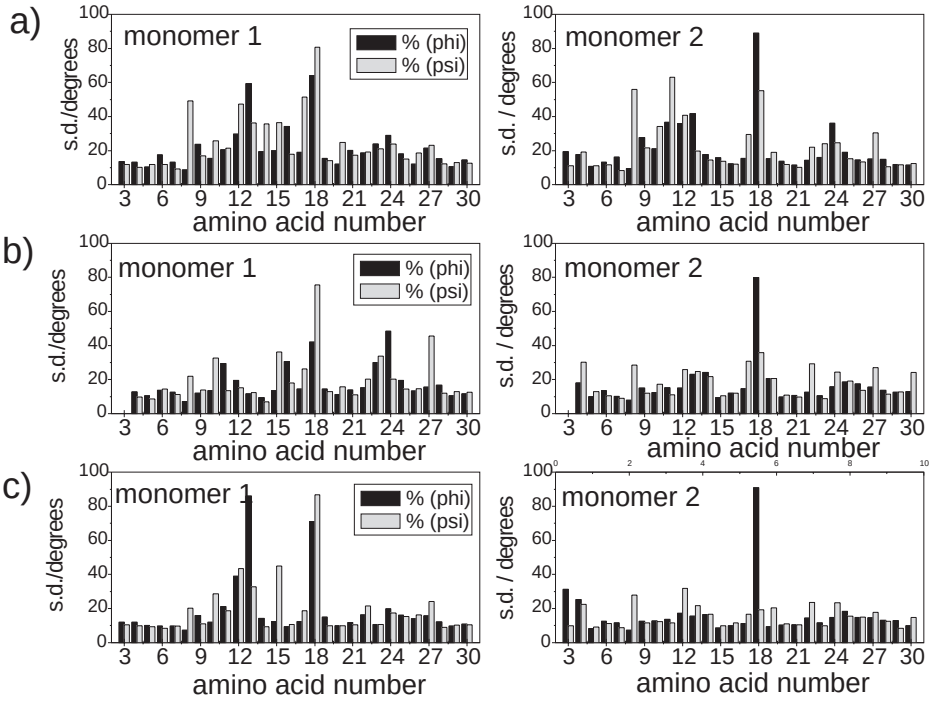

Figure 4. The standard deviations (s) calculated for the ϕ and ψ angles of each residue of the A: HNP-3, B: HNP-2 and C: HNP-1.

Table 2. The intramolecular hydrogen bonds identified in the HNPs, including the HB_{i-i} involving a) the backbone atoms ($HB_{back\text{-}back}$), b) the backbone and the side-chain atoms ($HB_{back\text{-}side}$) and c) the side-chain atoms ($HB_{side\text{-}side}$)

HNP-3				HNP-2				HNP-1			
$HB_{back\text{-}back}$											
Mon 1		Mon 2		Mon 1		Mon 2		Mon 1		Mon 2	
A-D[c]	%	A-D	%	A-D	%	A-D	%	A-D	%	A-D	%
4-30	92.0	4-30	98.6	4-30	97.9	18-29	93.6	4-30	98.8	4-30	97.6
6-28	71.4	6-28	50.3	6-28	59.3	22-25	37.9	6-28	63.6	11-16	48.3
18-29	97	15-31	72.1	12-17	79.3	27-20	98.7	16-31	57.2	13-16	33.8
22-25	37.5	20-27	70.7	13-16	69.1	28-10	41.9	18-29	98.1	15-31	82.9
27-20	95.2	27-20	97.3	17-12	56.6	29-17	91.9	20-27	76.4	18-29	98.7
28-6	95.6	28-6	93	17-15	12.1	29-18	69.8	27-20	99.7	20-27	74.7
30-4	76.8	29-17	94.5	28-6	92.1			28-6	98.8	27-20	99.4
		29-18	93.3	30-4	85.6			29-18	75	28-6	92.5
		30-4	98.2					30-4	74.2	29-17	94.3
										29-18	90.9
										30-4	94.0
$HB_{back\text{-}side}$[a]											
Mon 1		Mon 2		Mon 1		Mon 2		Mon 1		Mon 2	
A-D	%	A-D	%	A-D	%	A-D	%	A-D	%	A-D	%
11-**16**	29.3	**14**-15	42.8	**14**-15	44.7			**2-31**[b]	19.7	**14**-15	44.7
13-**16**	40.1			**14**-17	36.7			8-**6**	47.9	**14**-17	36.7
14-15	13.1			27-**19**	10.2			14-**16**	43.2	27-**19**	10.2
14-**16**	47.8			**31**-16	50.3			**31**-3	44.1	**31**-16	50.3
30-**6**	14.8							**31**-15	27.1		
31-4	23.8										
$HB_{side\text{-}side}$											
Mon 1		Mon 2		Mon 1		Mon 2		Mon 1		Mon 2	
A-D	%	A-D	%	A-D	%	A-D	%	A-D	%	A-D	%
										17-15	12.1

[a] the amino acid number in boldface indicates that it participates of the HB with the side-chain atom; [b] salt bridge; [c] A=acceptor, D=donor

show that each HNP have distinct stabilization by this mode of interaction. A total of 29, 18 and 23 HB_{i-i} were detected in the HNP-1, HNP-2 and HNP-3, respectively. The higher number of HB connecting the β-strands in the HNP-1 and HNP-3 and the lower number of these interactions in the HNP-2 reflects their flexibility as indicated by the RMSD values (Figure 3). A salt bridge detected between the N-terminus and the Asp2 carboxylate group in the monomer B of the HNP-1, despite of the low occurrence percentage, also contributes to the peptide stabilization.

Hydrogen bonds between the monomers

The HB formed between the atoms of each monomer of the dimeric defensin ($HB_{mon1\text{-}mon2}$) were computed using the same criteria for the HB_{i-i} described above. Hill *et al.*[13] observed four $HB_{mon1\text{-}mon2}$ in the HNP-3 crystalline structure (Table 3). During the simulations, others $HB_{mon1\text{-}mon2}$ were found in all defensins. Table 3 displays the $HB_{mon1\text{-}mon2}$ found in each HNP. The HNP-3 presents the major number of these interactions and, differently of the two other defensins, charged atoms are involved in these HB including a salt bridge between the side-chain atoms of the Asp^2 and Arg^6 residues (low occurrence). In general, the number of observations with occurrence percentage greater than 50% is the same for all the HNPs. The HNP-2 presents the minor number $HB_{mon1\text{-}mon2}$, indicating that the quaternary structure of this peptide is the less stabilized by these types of interactions at the interface. Two $HB_{mon1\text{-}mon2}$ are found in all the three defensins linking the two monomers at their amino termini, increasing the contacts in the β1-strand region of the monomers.

Table 3. Percentages of occurrence of the identified inter-monomers hydrogen bonds in the MD simulations of the HNP-3, HNP-2 and HNP-1 and the corresponding involved regions. The inter-monomers hydrogen bonds found in the X-ray structure are indicated

Mon 1		Mon 2		%	Regions
HNP-3					
Asp2	(OD1/2)	Arg6	(HE)	33	N term-β1
Asp2	(OD1)	Ile7	(NH)	25	N term-β1
Asp2	(OD2)	Arg6	(HH2)	25	N term-β1
Cys3	(NH)	Cys5	(CO)	37	β1-β1
Cys3	(CO)	Cys5	(NH)	96	β1-β1
Tyr4	(HH)	Asp2	(OD1/2)	31	β1-N term
Cys5	(NH)	Cys3	(CO)	89	β1-β1
Thr19	(CO)	Ile21	(NH)	79	β2-β2
Ile21	(NH)	Thr19	(CO)	52	β2-β2
Gln23	(NH)	Tyr17	(OH)	34	turn II-turn I
HNP-2					
Cys3	(CO)	Cys5	(NH)	98	β1-β1
Cys5	(NH)	Cys3	(CO)	97	β1-β1
Thr19	(CO)	Ile21	(NH)	88	β2-β2
Ile21	(NH)	Thr19	(CO)	94	β2-β2
HNP-1					
Cys3	(CO)	Cys5	(NH)	85	β1-β1
Cys5	(NH)	Cys3	(CO)	69	β1-β1
Arg16	(HH1)	Tyr22	(OH)	27	β2-β2
Thr19	(CO)	Ile21	(NH)	94	β2-β2
Ile21	(NH)	Thr19	(CO)	93	β2-β2
Gln23	(NH)	Tyr17	(CO)	34	turn II-turn I
HNP-3 crystal [13]					
Thr19	(CO)	Ile21	(NH)	-	β2-β2
Ile21	(NH)	Thr19	(CO)	-	β2-β2
Thr19	(NH)	Ile21	(CO)	-	β2-β2
Ile21	(CO)	Thr19	(NH)	-	β2-β2

Interaction potential energy

The potential energy for the interaction between the atoms of each monomer in the dimer was calculated for each defensin from the MD trajectories. Four types of interaction energies were computed: a) the interaction energy between the backbone atoms of the mon 1 and the backbone atoms of the mon 2 ($E_{back\text{-}back}$), b) the interaction energy values between the backbone atoms of one monomer with the side-chains atoms of the other monomer ($E_{back\text{-}side}$), c) the interaction energy between the side-chain atoms of each monomer ($E_{side\text{-}side}$) and d) the interaction energy between each peptide and the CCl_4 ($E_{peptide\text{-}CCl_4}$), (Figure 5).

The $E_{back\text{-}back}$ values for the HNP-3, Figure 5A, are very attractive during all time of simulations. The HNP-1 shows similar behavior to the HNP-3 until 5.4 ns, when a pronounced increase (~ –2 kcal/mol) followed by a decrease (~ –19 kcal/mol) in the energy values in the final of the simulations is observed. The HNP-2 energy values show a decrease in the first 0.86 ns and increase until ~ 2 kcal/mol, remaining repulsive until the end of the simulations.

The $E_{back\text{-}side}$, Figure 5B, oscillate around -23 kcal/mol and remain attractive along the simulations in all the cases. The profile of the $E_{side\text{-}side}$, Figure 5C, indicates repulsive interactions between the monomers of HNP-1 and between the monomers of HNP-2 (~ 125 kcal/mol) during the all time of simulations. For the HNP-3, repulsive interactions are observed in the beginning of the simulations (until 0.7 ns) and, after this, a pronounced decrease in the energy values which stabilize after 1.2 ns at ~ –50 kcal/mol occurs, showing attractive interactions between the side-chains of the monomers of HNP-3.

The energy for the interactions between the HNPs and the CCl_4, $E_{peptide\text{-}CCl_4}$, presents negative values (Figure 5D), indicating a favorable contact between all defensins and the hydrophobic medium.

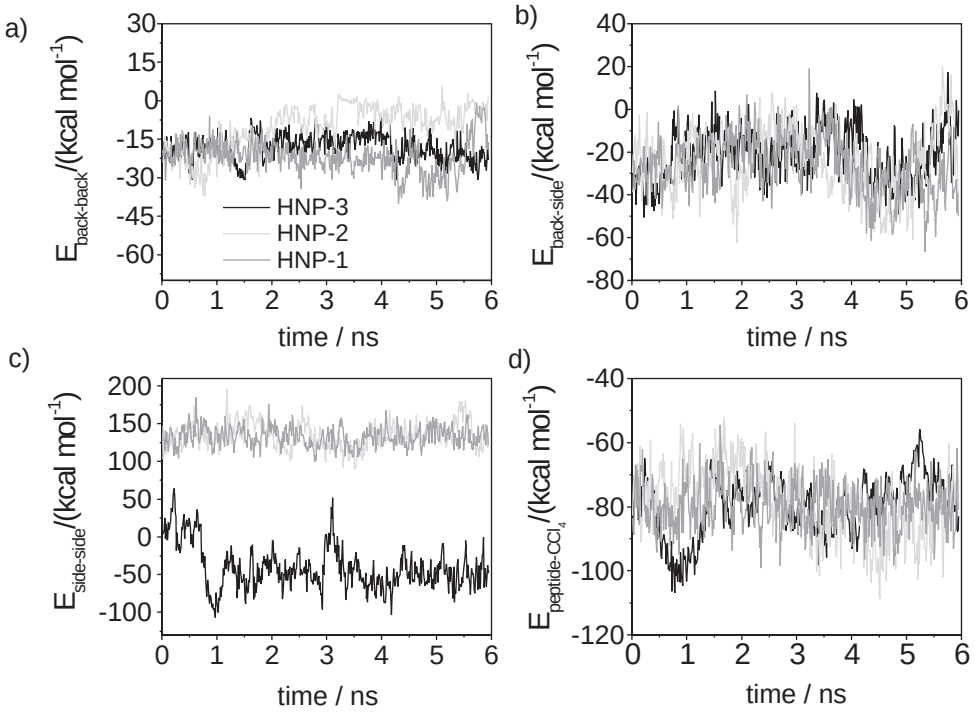

Figure 5. A: the interaction energy between the backbone atoms of the mon 1 and the backbone atoms of the mon 2 ($E_{back\text{-}back}$), B: the interaction energy values between the backbone atoms of one monomer with the side-chains atoms of the other monomer ($E_{back\text{-}side}$), C: the interaction energy between the side-chain atoms of each monomer ($E_{side\text{-}side}$) and D: the interaction energy between each peptide and the CCl_4 ($E_{peptide\text{-}CCl_4}$).

Hydration analyses

The numbers of water neighbors, N_w, in the first hydration shell of the peptide atoms are shown in Table 4 for each residue of the HNPs. These results indicate the regions exposed, or not, to the polar solvent. The mon 2 is more exposed to the aqueous solvent than the mon 1 in all defensins. The majority of the residues that comprises the β2 and β3 strands has no contact with the water molecules, indicating that these regions are responsible by either the interaction with the hydrophobic phase, or either by the $HB_{i\text{-}i}$ formation. In addition, these results show a very distinct behavior in the hydration of the CO and NH atoms: a greater number of CO atoms are in contact with the aqueous phase. The $n_{i,HB}$ obtained from the pair energy distributions, $d_i(E)$ for residue of the backbone atoms of three defensins are displayed in Figure 6. These results show that the responsible for the distinct solvation of the two monomers is the distinct hydration of the backbone atoms, since the number of hydration of side-chain atoms is very similar for the both monomers in all the three defensins (Figure 7). As seen in Table 4, all amino acids of mon 1 that comprise the hydrophobic basket bottom are totally isolated from the water molecules in all HNPs. On the other hand, some of them in the mon 2 (Gly24 and Leu26) are in contact with the aqueous medium, showing that the first contact between the dimer and the membrane hydrophobic phase occurs through mon 1.

Discussion

The present study provides information about the behavior of the human defensins at the membrane interface.

The RMSD values, displayed in the Figure 3, indicate that the defensins do not suffer denaturation at the interface. Their secondary structures, characterized in the initial configuration, are kept along of the simulations: this is confirmed by the low values of the standard deviations (s) for the ϕ and ψ angles. Four $HB_{mon1\text{-}mon2}$ (CO_{cys3}(mon1)-NH_{cys5}(mon2), NH_{cys5}(mon1)-CO_{Cys3}(mon2), CO_{Thr19}(mon1)-NH_{Ile21}(mon2) and NH_{Ile21}(mon1)-CO_{Thr19}(mon2)), are remained during the simulations in all HNPs, showing that the quaternary structures of the defensins are unaffected by the contact with the interface. The maintenance of the defensins dimeric structures suggests that they are able to form pores during the cellular membrane attack, once the dimerization is a prerequisite to this action. The final configuration for the HNP-3 at the interface is shown in the Figure 8.

Table 4. The number of water neighbors for all the residues of HNP-1, HNP-2 and HNP-3, obtained from the $g_i(r)$

Residue	HNP-3		HNP-2		HNP-1		Strand
	Mon 1	Mon 2	Mon 1	Mon 2	Mon 1	Mon 2	
Asp2	8.86	9.07	-	-	3.56	3.28	
Cys3	0.72	0.93	3.60	3.49	1.19	1.32	β1
Tyr4	1.77	1.58	3.33	2.26	2.63	2.14	β1
Cys5	1.28	0.67	1.35	1.17	1.24	1.08	β1
Arg6	4.49	3.20	4.66	4.04	4.76	4.57	β1
Ile7	1.81	1.36	1.65	1.85	1.94	1.87	β1
Pro8	0.70	0.73	0.85	0.85	0.79	0.51	
Ala9	0.42	1.28	0.56	2.00	0.57	0.41	
Cys10	0.40	0.70	0.63	0.43	0.46	0.52	
Ile11	1.0	1.38	0.95	2.02	1.14	0.88	
Ala12	0.59	1.86	0.69	2.11	0.86	1.14	
Gly13	0.87	2.16	0.92	2.08	0.66	1.93	
Glu14	8.01	7.50	8.69	7.97	8.33	7.71	
Arg15	5.09	5.75	4.22	4.18	5.17	4.08	
Arg16	4.64	5.48	3.78	4.98	5.49	5.26	
Tyr17	1.74	2.82	1.17	2.85	1.77	2.56	
Gly18	0	0	0	0	0	0	β2
Thr19	0	1.63	0	0.77	0	0	β2
Cys20	0	0	0	0	0	0	β2
Ile21	0	0	0	0	0	0	β2
Tyr22	2.00	1.95	1.84	1.69	1.93	1.89	β2
Gln23	2.52	2.41	2.99	2.30	2.37	1.89	
Gly24	0	0.88	0	0.98	0	0.49	
Arg25	3.01	4.41	3.99	5.20	4.12	5.27	β3
Leu26	0	2.16	0	1.61	0	0.96	β3
Trp27	0	0	0	0	0	0.41	β3
Ala28	0	0	0	0	0	0	β3
Phe29	0	0	0	0	0	0	β3
Cys30	0.71	0	0.98	0.75	0.71	0.49	β3
Cys31	7.05	6.74	6.18	5.82	7.07	6.77	

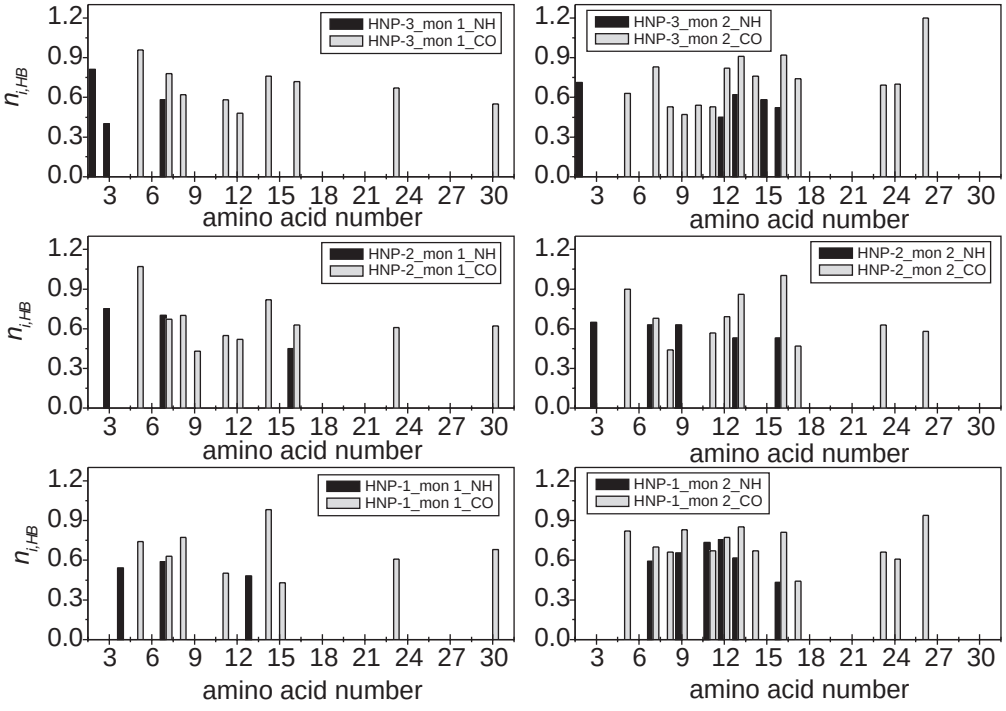

Figure 6. Hydration numbers from $g_i(r)$ for the CO and NH backbone atoms.

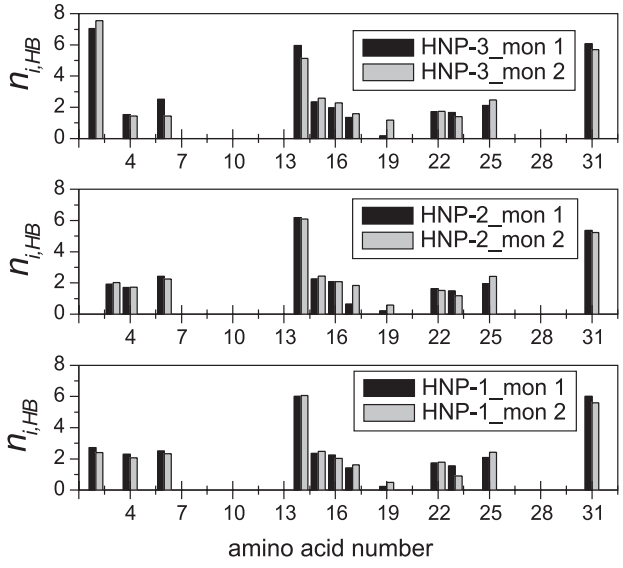

Figure 7. Hydration numbers from $g_i(r)$ for the polar side-chain atoms.

Figure 8. The final configuration of HNP-3 at the biphasic H_2O/CCl_4 system.

The $E_{side\text{-}side}$ attractive values found for the HNP-3 (around –50kcal/mol) are consistent with the higher number of $HB_{mon1\text{-}mon2}$ observed for this peptide, when compared with the HNPs 1 and 2. The higher number of $HB_{mon1\text{-}mon2}$ in the HNP-3 provides an increase of the hydrophobic core stability in the inner region of the dimer, formed by the Cys3, Cys5, Cys20, Tyr22, Trp27 and Phe29 amino acids (Figure 9A). This stabilization seems to hinder the interaction of the non-polar amino acids with the hydrophobic medium. On the other hand, the low number of the inter-monomers HB detected in the HNP-1 and HNP-2 can allow the entrance of water molecules in the interior of the dimer, leading to the migration of the hydrophobic groups towards the hydrophobic phase to compensate the loss of the stability.

The hydration analyses at the interface show that the mon 2 of each defensin is more hydrated than the mon 1, indicating that the contact between the peptide and the membrane hydrophobic phase occurs through monomer 1. The majority of the residues that are isolated from the water contact comprised the β2 and β3-strands.

The number of water neighbors for each residue calculated from the radial distribution functions (Table 1) show that the HNP-1 and the HNP-3 have a hydrophobic gain over the HNP-2, which can be explained by the stability of the hydrophobic core described above. On the other hand, considering the amino acids without water neighbors, only the HNP-2 possesses amino acids (Gly18, Cys20, Gly24, Leu26, Trp27 and Phe29 residues of the monomer 1) that do not participate of intramolecular HB and probably are in contact with the hydrophobic medium. In this way, the HNP-2 seems to present a better interaction with the hydrophobic medium when compared with the other two defensins. In all HNPs, the side chains of the Tyr4, Arg6, Glu14, Arg15, Arg16, Tyr17, Tyr22, Gln23 and Arg25 amino acids and the $–NH3^+$ and $–COO^-$ groups of N– and C– terminal, respectively, are highly hydrated by water molecules. Among these polar amino acids, the Glu14, Arg15, Arg16, Tyr17, Gln23, Arg25 (component of the β-turns) and the Tyr22 (component of the β2-strand) are occupying the interfacial region (Figure 9B), being possible candidates to promote the contacts between the defensin and the biological membrane.

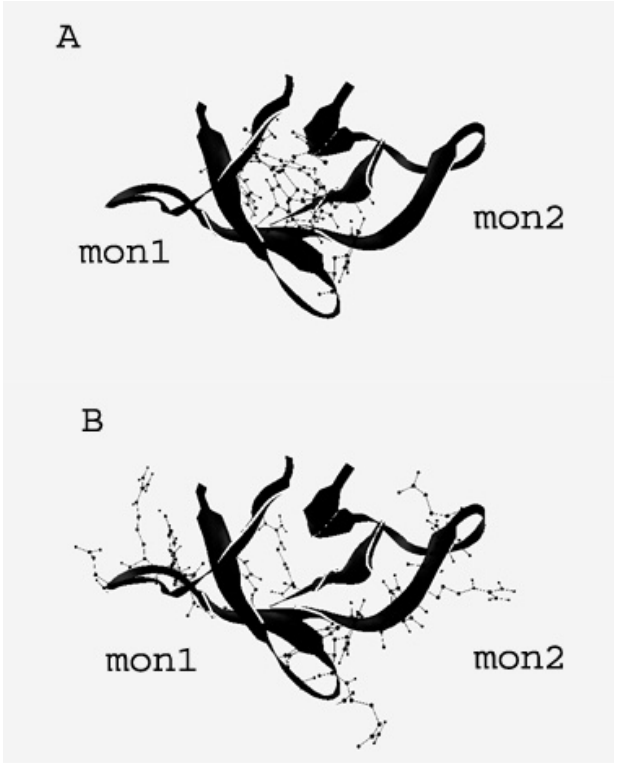

Figure 9. A: The hydrophobic core in the inner part of the HNP-3, formed by the Cys3, Cys5, Cys20, Tyr22, Trp27 and Phe29 amino acids, B: The polar amino acids, Glu14, Arg15, Arg16, Tyr17, Tyr22, Gln23 and Arg25, in the HNP-3, that are occupying the interfacial region.

Conclusions

Our studies show that the human defensins HNP-1, HNP-2 and HNP-3 do not lose their dimeric structures at the interface. The hydrophobic core stability in the inner region of the dimer, largely due to the interactions with the CCl_4 phase that mimic the hydrophobic inner part of the cellular membranes, can be a motive for the extension of the HNP activities. The HNP-3 is the least potent of the three defensins studied and it is also the dimer that presents the higher stability of its hydrophobic core. Their apolar residues cannot make the membrane attack because they are shielded in the inner region of the peptide, differently from the HNPs 1 and 2.

The results presented here show that the stability and orientation of the HNPs at the interface agree with the prerequisite for membrane binding and pore formation suggested in the literature,[13,31] since their dimeric structures remain stable when in contact with the interface.

Acknowledgments

The authors thank the Fundação de Amparo à Pesquisa do Estado de São Paulo (FAPESP) and the Conselho Nacional de Desenvolvimento Científico e Tecnológico (CNPq) for financial support.

References

1. Hancock, R. E. W.; Diamond, G.; *Trends Microbiol.* **2000**, *8*, 402.
2. Hughes, A. L.; *Cell. Mol. Life Sci.* **1999**, *56*, 94.
3. Hancock, R. E. W.; Lehrer, R.; *Trends Biotech.* **1998**, *16*, 82.
4. Epand, R. M.; Vogel, H. J.; *Biochim. Biophys. Acta* **1999**, *1462*, 11.
5. Bechinger, B.; *Biochim. Biophys. Acta* **1999**, *1462*, 157.
6. Matsuzaki, K.; *Biochim. Biophys. Acta* **1998**, *1376*, 391.
7. Kleinkauf, H.; von Döhren H. Eds.; *Biochemistry of Peptide Antibiotics*, Walter de Gruyter: Berlin, 1990.
8. Oren, Z.; Shai, Y.; *Biopolymers* **1998**, *47*, 451.
9. Ganz, T.; Lehrer, R. I.; *Pharmacol. Ther.* **1995**, *66*, 191.
10. Rice, W. G.; Ganz, T.; Kinkade Jr., J. M.; Selsted, M. E.; Parmley, R. T.; *Blood* **1987**, *70*, 757.
11. Selsted, M. E.; Harwig, S. S.; Ganz, T.; Schilling, J. W.; Lehrer, R. I.; *J Clin Invest.* **1985**, *76*, 1436.
12. Pardi, A.; Zhang, X. L.; Selsted, M. E.; Skalicky, J. J.; Yip, P. F.; *Biochemistry* **1992**, *31*, 11357.
13. Hill, C. P.; Yee, J.; Selsted, M. E.; Eisenberg, D.; *Science* **1991**, *251*, 1481.
14. White, S. H.; Wimley, W. C.; Selsted, M. E.; *Curr. Opin. Struct.* **1995**, *5*, 521.
15. Ganz, T.; Selsted, M. E.; Szklarek, D.; Harwig, S. S.; Daher, K.; Bainton, D. F.; Lehrer, R. I.; *J. Clin. Invest.* **1985**, *76*, 1427.
16. Daher, K. A.; Selsted, M. E.; Lehrer, R. I.; *J. Virol.* **1986**, *60*, 1068.
17. Lehrer, R. I.; Ganz, T.; Szklarek, D.; Selsted, M. E.; *J. Clin. Invest.* **1988**, *81*, 1829.
18. Shafer, W. M.; Engle, S. A.; Martin, L. E.; Spitznagel, J. K.; *Infect. Immun.* **1988**, *56*, 51.
19. Miyasaki, K. T.; Bodeau, A. L.; Ganz, T.; Selsted, M. E.; Lehrer, R. I.; *Infect. Immun.* **1990**, *58*, 3934.
20. Ogata, K.; Linzer, B. A.; Zuberi, R. I.; Ganz, T.; Lehrer, R. I.; Catanzaro, A.; *Infect. Immun.* **1992**, *60*, 4720.
21. Aley, S. B.; Zimmerman, M.; Hetsko, M.; Selsted, M. E.; Gillin, F. D.; *Infect. Immun.* **1994**, *62*, 5397.
22. Turchany, J. M.; Aley, S. B.; Gillin, F. D.; *Infect. Immun.* **1995**, *63*, 4550.
23. Miyakawa, Y.; Ratnakar, P.; Rao, A. G.; Costello, M. L.; Mathieu-Costello, O.; Lehrer, R. I.; Catanzaro, A.; *Infect. Immun.* **1996**, *64*, 926.
24. Yasin, B.; Harwig, S. S.; Lehrer, R. I.; Wagar, E. A.; *Infect. Immun.* **1996**, *64*, 709.
25. Turner, J.; Cho, Y.; Dinh, N. N.; Waring, A. J.; Lehrer, R. I.; *Antimicrob. Agents. Chemother.* **1998**, *42*, 2206.
26. Newman, S. L.; Gootee, L.; Gabay, J. E.; Selsted, M. E.; *Infect. Immun.* **2000**, *68*, 5668.
27. Mackewicz, C. E.; Yuan, J.; Tran, P.; Diaz, L.; Mack, E.; Selsted, M. E.; Levy, J. A.; *AIDS* **2003**, *17*, F23.
28. *Chang, T. L.; Klotman, M. E.;* AIDS Rev. ***2004****, 6, 161-168.*
29. Bastian, A.; Schafer, H.; *Regul. Pept.* **2001**, *101*, 157.
30. Chang, T. L.; Vargas, J.; DelPortillo, A.; Klotman, M. E.; *J Clin Invest.* **2005**, *115*, 765.
31. Wimley, W. C.; Selsted, M. E.; White, S. H.; *Protein Sci.* **1994**, *3*, 1362.
32. Fujji, G.; Selsted, M. E.; Eisenberg, D.; *Protein Sci.* **1993**, *2*, 1301.
33. Namba, A. M.; Degréve, L.; *Quim. Nova* **2004**, *27*, 27.
34. Degrève, L.; Brancaleoni, G. H.; Fuzo, C. A.; Lourenzoni, M. R.; Mazzé, F. M.; Namba, A. M.; Vieira, D. S.; *Braz. J. Phys.* **2004**, *34*, 102.
35. Guba, W.; Kessler, H.; *J. Phys.Chem.* **1994**, *98*, 23.
36. Mercurio, E.; Pellegrini, M.; Mierke, D. F.; *Biopolymers* **1997**, *42*, 759.
37. Wymore, T.; Wong, T. C.; *Biophys. J.* **1999**, *76*, 1199.
38. van Gunsteren, W. F.; Billeter, S. R.; Eising, A. A.; Hünenberger, P. H.; Krüger, P. K.; Mark, A. E.; Scott, W. R. P.; Tironi, I. G.; *Biomolecular Simulation: The GROMOS96 Manual and User Guide*, Verlag der Fachvereine: Switzerland, 1996.
39. Berendsen, H. J. C.; Grigera, J. R.; Straatsma, T. P.; *J. Phys. Chem.* **1987**, *91*, 6269.
40. Tironi, I. G.; Sperb, R.; Smith, P. E.; van Gunsteren, W. F.; *J. Chem. Phys*. **1995**, *102*, 5451.

41. Allen, M. P.; Tildesley, D. J.; *Computer Simulation of Liquids*, Claredon Press: Oxford, 1987.
42. Cicotti, G.; Frenkel, D.; McDonald, I. R.; *Simulation of Liquids and Solids. Molecular Dynamics and Monte Carlo Methods in Statistical Mechanics*, North-Holland: Amsterdam, 1990.
43. Ryckaert, J. P.; Ciccotti, G.; Berendsen, H. J. C.; *J. Comput. Phys.* **1977**, *23*, 327.
44. Ramachandran, G. N.; Sasisekharan, V.; *Adv. Protein Chem.* **1968**, *23*, 283.
45. Jorgensen, W. L.; Chandrasekhar, J.; Madura, J. D.; Impey, R. W.; Klein, M. L.; *J. Chem. Phys.* **1983**, *79*, 926.

Received: July 1, 2005
Web Release Date: May 15, 2007

FAPESP helped in meeting the publication costs of this article.